

# A higher-order boundary layer analysis for lipid vesicles with two fluid domains

SOVAN L. DAS<sup>†</sup> AND JAMES T. JENKINS

Theoretical and Applied Mechanics, Cornell University, Ithaca, NY 14853, USA

(Received 26 August 2007 and in revised form 13 November 2007)

We obtain approximate solutions to the equations that govern the shape of giant unilamellar vesicles (GUVs) with two fluid phases. The equations involve a dimensionless small parameter related to the resistance to changes in its local mean curvature. Asymptotic solutions for the shape are obtained up to and including terms of first order in the small parameter. At this order, we determine a relationship between the tangent angle at the interface and the difference in the Gaussian curvature stiffnesses of the co-existing phases. This relationship demonstrates that a difference in the Gaussian curvature stiffnesses moves the phase boundary away from the neck, as determined in previous numerical studies. The analytical expression for the tangent angle obtained here can be used to determine elastic parameters for the membranes from experimental data. Use of the analytical expression will eliminate the need for the repeated generation of numerical solutions in the estimation of the material parameters. Our analytical solution also reduces the number of measurements needed as inputs for an existing boundary layer analysis.

---

## 1. Introduction

The biological membranes of animal cells are complicated bilayer structures composed of different types of phospholipid molecules, cholesterol, and proteins (Israelachvili 1992; Lipowsky & Sackmann 1995; Alberts *et al.* 2002; Leibler 2004). Because of their complicated structure, a systematic study of mechanical or thermal behaviour of a biological membrane is difficult. However, lipid bilayer vesicles are simpler, can be made in laboratories without much difficulty, and are easier to study. They consist of many of the same phospholipids that, in association with cholesterol, form cell membranes. They are fluid-like, spontaneously form in aqueous solution, resist bending, and have a large variety of shapes. Their sizes vary from about 20 nanometres to a few hundred micrometres in diameter, with thickness only a few nanometres. The giant unilamellar vesicles (GUVs) have sizes in the micrometre range and can be visualized using optical microscopes. Because of their large diameter-to-thickness ratio, they are modelled as surfaces in a three-dimensional space that are characterized locally by their mean and Gaussian curvatures (Helfrich 1973; Jenkins 1977; Evans & Yeung 1994; Seifert 1997; Leibler 2004).

When a GUV consists of two coexisting fluid domains (Baumgart, Hess & Webb 2003; Baumgart *et al.* 2005), it is deformed by the line tension associated with the energy of the thickness difference between coexisting domains (Akimov *et al.* 2004)

<sup>†</sup> Present address: Department of Mathematics, Pennsylvania State University, University Park, PA 16802, USA.

and the compositional inhomogeneity (Widom 1999) across the phase boundary. The deformation induced by the line tension is balanced by the bending resistance of the vesicle and the osmotic pressure difference across the membrane. However, for a stretched GUV, the resistance to bending is important only in a small region that contains the phase boundary (Allain & BenAmar 2006).

In this work, we carry out a boundary layer analysis to an order higher than in an existing analysis (Allain & BenAmar 2006). The existing analysis, to lowest order in the perturbation parameter, has been employed to predict the onset of budding and to estimate the contribution of the bending resistance to the effective line tension at the phase interface (Allain & BenAmar 2006). The lowest-order analysis of Allain & BenAmar (2006) consists of the complete outer layer solution, the inner layer solution for the tangent angle, and matching of inner and outer layers for the tangent angle. They do not obtain a complete inner layer solution and its matching with the outer layer. Here, we carry out the full solution, extend the analysis to higher order, include matching of the inner and outer solutions, and construct the composite solution. The full outer and inner layer solutions and their matching, at the lowest order, permits the shape to be described with fewer input parameters.

The extension to higher order incorporates the resistance of the vesicle to changes in Gaussian curvature, which cannot be captured by the lowest-order analysis. This resistance plays an important role in determining the geometry of a phase-separated vesicle near its neck. Using a numerical solution of the shape equations, its influence has been studied when a vesicle is close to budding (Jülicher & Lipowsky 1996; Lipowsky *et al.* 2005). It was observed that differing Gaussian curvature stiffnesses between the phases shift the phase boundary away from narrowest part of the neck. The relative magnitude of the Gaussian curvature stiffnesses determines whether the difference favours or hinders bud formation (Jülicher & Lipowsky 1996). For vesicles far away from budding, Baumgart *et al.* (2005) used numerical solutions to examine similar displacements of the phase boundary. The analytical solution that we obtain here exhibits such effects when the shapes are not close to budding. For budded shapes, a rescaling of the neck radius is necessary and this results in equations that are analytically intractable.

In addition to solving the differential equations for the shape separately in the regions near and away from the interface, we solve the jump conditions and equations obtained from asymptotic matching analytically at each order of the boundary layer analysis. The latter solution provides expressions for the geometric quantities that describe the overall shape of the vesicle, the line tension, and the tangent angle at the interface in terms of the mechanical properties, the amount of the coexisting phases, and the boundary radius of the interface. Moreover, the composite solution for tangent angle near the interface can be used to determine the relative magnitude of the Gaussian curvature stiffnesses, together with the line tension at the interface, using experimental vesicle data.

## 2. Equations and jump conditions

Figure 1 shows a schematic of the closed axisymmetric vesicle that we consider in the present work. The membrane consists of two phases, labelled (–) and (+). In reference to experimental vesicle shapes (Baumgart *et al.* 2005), the two phases correspond to liquid ordered ( $L_o$ ) and liquid disordered ( $L_d$ ) domains, respectively, and are assumed to be separated by a sharp interface. Although this is an idealization, GUVs prepared from ternary lipid mixtures of a low-melting-temperature lipid

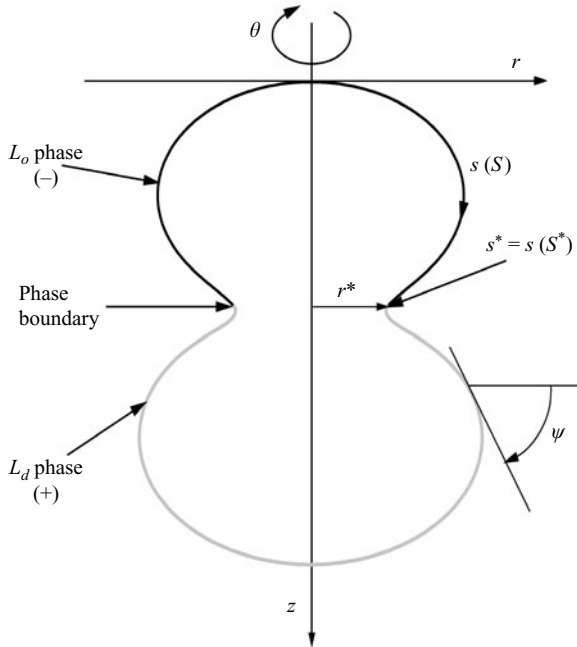


FIGURE 1. Parametrization of the two-phase membrane for an axisymmetric deformation. The initial configuration is taken to be a sphere of radius  $\rho$ . The  $(-)$  and  $(+)$  regions correspond to liquid ordered ( $L_o$ ) and liquid disordered ( $L_d$ ) domains, respectively (Baumgart *et al.* 2005).

such as dioleoylphosphatidylcholine (DOPC), high-melting-temperature lipids such as dipalmitoylphosphatidylcholine (DPPC) or egg sphingomyelin (ESM), and cholesterol exhibit a situation similar to that considered here (Almeida, Fedorov & Prieto 2003; Veatch & Keller 2003, 2005). This occurs at room temperature, which is far from the critical point, and when compositions of the mixtures lie in the  $L_o - L_d$  coexistence region of a ternary phase diagram. We also assume that the area occupied by each phase in a vesicle is not coupled to shape changes (Jülicher & Lipowsky 1996) and the temperature is constant. Then the chemical potential of the lipid components is constant and not coupled to shape changes. The bending stiffness of the membranes is typically of the order of  $10^{-19}$  N m (Evans 1980; Duwe, Käs & Sackmann 1990; Israelachvili 1992; Leibler 2004) and the area compression modulus of the membranes is of the order  $10^{-1}$  N m $^{-1}$  (Israelachvili 1992; Waugh & Evans 1979). The large difference in the order of magnitudes of these two moduli makes it significantly harder to induce changes in the area of membranes of GUVs than to bend them and the membranes are assumed to be laterally incompressible.

For a laterally incompressible fluid bilayer, with inner and outer monolayers indistinguishable and the long axis of the lipid molecules oriented along the direction normal to the membrane surface, the bending free energy per unit area has the form  $w = w(h^2, k)$ , where  $h$  and  $k$  are the mean and Gaussian curvatures of the membrane. The simplest form of  $w$  is

$$w = \kappa h^2 + \kappa_g k, \tag{2.1}$$

where  $\kappa$  and  $\kappa_g$  are the bending stiffnesses corresponding to the mean and Gaussian curvatures, respectively (Helfrich 1973; Jenkins 1976; Seifert 1997). The total bending energy is obtained by integrating  $w$  over the entire membrane area. For

a homogeneous vesicle with spherical topology, the integral of Gaussian curvature is constant (ONeil 1966) and the Gaussian curvature stiffness  $\kappa_g$  does not play a role. However, for a phase-separated membrane,  $\kappa_g$  does influence the shape through the jump conditions that relate the bulk equilibrium equations at the interface between the phases (Jülicher & Lipowsky 1996).

The equilibrium shape equations and jump conditions are obtained by minimizing the energy functional with contributions from the total bending energy, the line energy at the interface, and the pressure difference between the inside and outside of the vesicle (Jenkins 1977; Jülicher & Lipowsky 1996). Alternatively, they can be obtained through the balance of forces and moments on an infinitesimal area element of the membrane (Evans & Yeung 1994; Calladine & Greenwood 2002; Powers, Huber & Goldstein 2002). In the (−) region, the equations that govern the dimensionless transverse shear stress  $Q_s$  and mean curvature  $h$  (equations 18, 19 of Baumgart *et al.* (2005)) are

$$(Q_s)' + \frac{r' Q_s}{r} - 2h \left[ -d + \varepsilon h^2 + \varepsilon \frac{\sin \psi}{r} \left( 2h + \frac{\sin \psi}{r} \right) \right] = -p \quad (2.2)$$

and

$$h' = -Q_s/\varepsilon. \quad (2.3)$$

In the above, lengths are made dimensionless by the radius  $\rho$  of a reference sphere and forces are made dimensionless by the ratio of the mean curvature bending stiffness  $\kappa^+$  in the (+) region to  $\rho$ . The parameter  $\varepsilon \equiv \kappa^-/\kappa^+$  is the ratio between mean curvature bending stiffnesses of the (−) region  $\kappa^-$  and the (+) region  $\kappa^+$ . Changes in the tangent angle  $\psi$  and the distance of a point on the membrane from the axis of symmetry  $r$  (see figure 1) are governed by

$$\psi' = -2h - \frac{\sin \psi}{r}, \quad r' = \cos \psi. \quad (2.4)$$

Lateral incompressibility of the membrane is imposed by assuming that during deformation the vesicles preserve their local surface area. This gives

$$\varpi' \equiv (\cos S)' = -r, \quad (2.5)$$

where  $S$  is the arclength of the reference sphere made dimensionless by its radius  $\rho$ . The prime denotes derivative with respect to deformed arclength  $s$ ; and  $p$  and  $d$  are, respectively, the dimensionless inner excess pressure and the dimensionless mean lateral tension. The Lagrange multiplier  $\gamma(s)$  associated with the conservation of local area is given by (Jenkins 1976)

$$\gamma(s)r + \varepsilon h^2 = -d.$$

The mean lateral tension  $d$  is a constant that may be different in each phase. It corresponds to the Lagrange multiplier when a global area constraint is imposed (Helfrich 1973; Jülicher & Lipowsky 1996).

The introduction of the reference arclength, through (2.5), permits specification of the area fraction of each phase. This, in turn, allows the determination of the position of the interface and the radii of the outer spheres in terms of the area fraction.

For large pressures,  $\mu^2 \equiv 1/p$  is a small parameter (Allain & BenAmar 2006). We also define another dimensionless quantity  $\tau \equiv 2d/p$ . Then the nonlinear differential

equation for  $h$ ,

$$\mu^2 h'' + \frac{\mu^2 r' h'}{r} - h \left[ \frac{\tau}{\varepsilon} - 2\mu^2 \left( h^2 + 2h \frac{\sin \psi}{r} + \frac{\sin^2 \psi}{r^2} \right) \right] = \frac{1}{\varepsilon}, \tag{2.6}$$

is obtained by combining (2.2) and (2.3) and employing the dimensionless variables. The remaining differential equations from (2.4) and (2.5) are

$$\psi' = -2h - \frac{\sin \psi}{r}, \quad r' = \cos \psi, \quad \varpi' \equiv (\cos S)' = -r. \tag{2.7}$$

The equations in the (+) region are identical, except that the parameter  $\varepsilon$  is unity.

The quantities  $\psi$ ,  $r$ , and  $\varpi$  are continuous at the interface,  $s = s^*$ , where  $s^*$  must be determined:

$$\psi^- = \psi^+ = \psi^*, \quad r^- = r^+ = r^*, \quad \varpi^- = \varpi^+ = \varpi^*,$$

with  $\psi^*$ ,  $r^*$ , and  $\varpi^* = \cos S^*$  being the values of  $\psi$ ,  $r$ , and  $\varpi$  at the interface. The jump conditions for the transverse force, the tangential force, and the moment at the interface are (Jülicher & Lipowsky 1996; Baumgart *et al.* 2005)

$$Q_s^+ - Q_s^- - \hat{\sigma} \frac{\sin \psi^*}{r^*} = 0, \tag{2.8}$$

$$d^+ - d^- - [(h^+)^2 - \varepsilon (h^-)^2] - \Delta \frac{\sin^2 \psi^*}{r^{*2}} - \hat{\sigma} \frac{\cos \psi^*}{r^*} = 0, \tag{2.9}$$

$$h^+ - \varepsilon h^- - \Delta \frac{\sin \psi^*}{r^*} = 0, \tag{2.10}$$

where  $\hat{\sigma}$  is the dimensionless line tension and  $\Delta \equiv (\kappa_g^+ - \kappa_g^-)/k^+$  is a measure of the difference in the Gaussian curvature stiffnesses  $\kappa_g^-$  and  $\kappa_g^+$  in the two regions. Equations (2.8) and (2.9) can be rewritten in terms of the small parameter  $\mu$  as

$$\mu^2 [(h^+)' - \varepsilon (h^-)'] + \sigma \frac{\sin \psi^*}{r^*} = 0, \tag{2.11}$$

$$\frac{1}{2} (\tau^+ - \tau^-) - \mu^2 \left[ (h^+)^2 - \varepsilon (h^-)^2 + \Delta \frac{\sin^2 \psi^*}{r^{*2}} \right] - \sigma \frac{\cos \psi^*}{r^*} = 0, \tag{2.12}$$

where  $\sigma = \hat{\sigma}/p$  is the dimensionless line tension normalized by  $p$  and (2.10) remains unchanged. In contrast to Jülicher & Lipowsky (1996) and Allain & BenAmar (2006), we phrase the problem in terms of both  $h$  and  $\psi$  rather than  $\psi$  alone. This is because the jump conditions at the phase boundary are naturally expressed in terms of the two variables. Using the first of (2.7), the shape equations and boundary conditions can also be written in terms of the tangent angle  $\psi$  and its derivatives alone (Jülicher & Lipowsky 1996; Allain & BenAmar 2006).

The boundary conditions at the north pole,  $s = 0$ , are

$$(h^-)' = 0, \quad \psi^- = 0, \quad r^- = 0, \quad \varpi^- = 1. \tag{2.13}$$

The boundary conditions at the south pole,  $s = \hat{s}$ , where  $\hat{s}$  must be determined, are

$$(h^+)' = 0, \quad \psi^+ = \pi, \quad \varpi^+ = -1. \tag{2.14}$$

The condition  $r(\hat{s}) = 0$  is automatically satisfied by a solution of the shape equations subjected to the jump conditions and the boundary conditions at the poles (Jenkins 1976; Das 2007).

The experimentally measured quantities are the ratio  $\chi^+$  of the area of the (+) domain to the total membrane area and the boundary radius  $r^*$ . Also,

$$\chi^+ = \frac{1}{2}(1 + \varpi^*) \quad \text{which gives} \quad \varpi^* = 2\chi^+ - 1. \tag{2.15}$$

The other parameters that appear in the approximate analytical solution are  $s^*$ ,  $\hat{s}$ ,  $\tau^-$ ,  $\tau^+$ , and  $\sigma$ . They are determined from our analysis. Note that in a phase-separated vesicle, its lipid composition determines the line tension  $\sigma$ , which, in turn, determines the boundary radius. However, in experimental vesicle images, it is not possible to measure the line tension, but it is possible to measure  $r^*$ . Consequently, in our analysis,  $r^*$  is treated as a known parameter and  $\sigma$  is solved for. This allows estimation of the line tension from equilibrium shape analysis. A similar approach has also been discussed in Baumgart *et al.* (2005).

### 3. Boundary layer

The mean curvature bending stiffness  $\kappa$  is small compared to  $\bar{p}\rho^3$ , where  $\bar{p}$  is the pressure in physical units. For example, the vesicle analysed by Baumgart *et al.* (2005) gives  $\bar{p} \approx 10^{-2} \text{ N m}^{-12}$  and  $\rho \approx 9.8 \text{ }\mu\text{m}$ , resulting in  $\bar{p}\rho^3 \approx 10^{-17} \text{ N m}$  and, as mentioned earlier,  $\kappa$  is of the order  $10^{-19} \text{ N m}$  (Duwe *et al.* 1990). As a result, the factor  $\mu$  appearing in (2.6) is very small (Allain & BenAmar 2006). For zero bending resistance, the shape of the vesicle under the action of a line tension at the interface resembles two truncated spheres with a kink at their circle of intersection. Small non-zero bending stiffness eliminates the discontinuity in tangent angle at the interface, but does not change the global shape much. The kink at the interface is then replaced by a narrow region in which there is a rapid change in the tangent angle, resulting in large longitudinal curvature. This region of rapid change is the boundary layer (Hinch 1991; Bender & Orszag 1999; Powers *et al.* 2002; Allain & BenAmar 2006). Here, we describe a boundary layer calculation that includes terms of order  $\mu$ . The lowest-order and order- $\mu$  analyses are also referred as order one and first order, respectively. The lowest-order solution for the tangent angle was obtained by Allain & BenAmar (2006). We provide complete lowest-order solutions for the outer and inner layers in Appendices A and B, respectively.

#### 3.1. Outer layer

We first describe the analysis for the (−) region. The outer layer is the region away from the interface, where the membrane has constant curvature. In this region, a regular perturbation expansion of the variables in the small parameter  $\mu$  (Hinch 1991) is

$$h = h_0 + \mu h_1, \quad \psi = \psi_0 + \mu \psi_1, \quad r = r_0 + \mu r_1, \quad \varpi = \varpi_0 + \mu \varpi_1, \quad \tau = \tau_0 + \mu \tau_1. \tag{3.1}$$

Using the expansions given in (3.1), at the order  $\mu$ ,

$$h_1 = \frac{\tau_1}{\tau_0^2}, \quad \psi_1' = -\frac{2\tau_1}{\tau_0^2} - \frac{\psi_1}{\tau_0} \cot \frac{s}{\tau_0} + \frac{r_1}{\tau_0^2 \sin(s/\tau_0)}, \tag{3.2}$$

$$r_1' = -\sin \frac{s}{\tau_0} \psi_1, \quad \varpi_1' = -r_1. \tag{3.3}$$

The solution of the system of equations (3.2) and (3.3) with boundary conditions  $\psi_1(0) = 0$ ,  $r_1(0) = 0$ , and  $\varpi_1(0) = 0$  is

$$\psi_1 = -\frac{\tau_1}{\tau_0^2} s, \quad r_1 = \tau_1 \sin \frac{s}{\tau_0} - \frac{\tau_1 s}{\tau_0} \cos \frac{s}{\tau_0},$$

$$\varpi_1 = 2\tau_1 \tau_0 \left( \cos \frac{s}{\tau_0} - 1 \right) + \tau_1 s \sin \frac{s}{\tau_0}.$$

Using expressions from Appendix A, the outer solution, including terms of order  $\mu$ , is given by

$$h = -\frac{1}{\tau_0} + \mu \frac{\tau_1}{\tau_0^2}, \quad \psi = \frac{s}{\tau_0} - \mu \frac{\tau_1}{\tau_0^2} s, \quad r = \tau_0 \sin \frac{s}{\tau_0} + \mu \left( \tau_1 \sin \frac{s}{\tau_0} - \frac{\tau_1 s}{\tau_0} \cos \frac{s}{\tau_0} \right),$$

$$\varpi = \tau_0^2 \left( \cos \frac{s}{\tau_0} - 1 \right) + 1 + \mu \left[ 2\tau_1 \tau_0 \left( \cos \frac{s}{\tau_0} - 1 \right) + \tau_1 s \sin \frac{s}{\tau_0} \right].$$

Note that the outer layer up to order  $\mu$  is a spherical cap of radius  $\tau_0 - \mu(\tau_0^2/\tau_1)$ .

### 3.2. Inner layer

The inner layer is the narrow region around the interface. As mentioned before, curvature changes rapidly in this region. A typical value of the line tension is  $\bar{\sigma} \approx 10^{-12}$  N, so the dimensionless line tension  $\sigma \equiv \bar{\sigma}/(\bar{p}\rho^2)$  is of order one. The lowest-order outer layer solution for  $h$  indicates that the ratio of mean lateral tension and pressure  $\tau$  is also of order one. Moreover, we focus on vesicles for which the radius  $r$  near the interface is of order one. With these, the dominant terms in (2.6) and jump condition (2.11) arise from the contributions of the mean lateral tension ( $h\tau/\varepsilon$ ) and the line tension ( $\sigma \sin \psi^*/r^*$ ), respectively. These are balanced by the bending terms of the corresponding equations when  $s$  and  $h$  are scaled as

$$\xi = \frac{s - s^*}{\mu}, \quad h = \frac{H}{\mu},$$

where  $s^*$  is the arclength at the phase boundary. Then  $\xi$  and  $H$  are the stretched arclength and the scaled mean curvature, respectively. These are equivalent to the scalings used in the earlier boundary layer analyses (Powers *et al.* 2002; Allain & BenAmar 2006).

During budding and fission, the neck becomes extremely thin, so  $r$  is of order  $\mu$  rather than order one. Consequently, our analysis does not apply in this case. Allain & BenAmar (2006) predicted the onset of budding by comparing energies of vesicles with different boundary radius and the same normalized line tension  $\sigma$ . However, they do not describe budded shapes that require the rescaling of  $r$  in the neck region. Upon considering  $r$  to be of order  $\mu$  we find that, unlike (B 1), the lowest-order equations obtained from (3.4) and (3.5) are nonlinear and coupled, and finding an analytical solution is not feasible. This was also observed by Powers *et al.* (2002) in the context of tether formation.

In the (−) region,  $s \leq s^*$ , resulting in  $\xi \leq 0$ . In terms of the stretched variable, the shape equations are

$$\ddot{H} - \frac{\tau}{\varepsilon} H + 2H^3 + \mu 2H \frac{\sin \psi}{r} \left( 2H + \mu \frac{\sin \psi}{r} \right) + \mu \frac{\cos \psi}{r} \dot{H} = \frac{\mu}{\varepsilon}. \quad (3.4)$$

$$\dot{\psi} = -2H - \mu \frac{\sin \psi}{r}, \quad \dot{r} = \mu \cos \psi, \quad \dot{\varpi} = -\mu r, \quad (3.5)$$

where the overdot denotes a derivative with respect to  $\xi$ .

We now assume the perturbation expansion

$$H = H_0 + \mu H_1 + \mu^2 H_2, \quad \psi = \psi_0 + \mu \psi_1, \quad r = r_0 + \mu r_1,$$

$$\varpi = \varpi_0 + \mu \varpi_1, \quad \tau_0 = \tau_0 + \mu \tau_1 + \mu^2 \tau_2.$$

The solution at the lowest order is given in Appendix B. At order  $\mu$ , the equations are

$$\begin{aligned} \ddot{H}_1 - \left( \frac{\tau_0}{\varepsilon} - 6H_0^2 \right) H_1 &= \frac{1}{\varepsilon} + \frac{\tau_1}{\varepsilon} H_0 - 4H_0^2 \frac{\sin \psi_0}{r^*} - \dot{H}_0 \frac{\cos \psi_0}{r^*}, \\ \dot{\psi}_1 &= -2H_1 - \frac{\sin \psi_0}{r^*}, \quad \dot{r}_1 = \cos \psi_0, \quad \dot{\varpi}_1 = -r^*. \end{aligned}$$

The solution at this order is given by

$$\begin{aligned} H_1 &= \left[ A + \frac{2N}{r^*} \arctan(\sinh \zeta) + \frac{4M}{r^*} \ln(\operatorname{sech} \zeta) \right] \operatorname{sech} \zeta \tanh \zeta - \frac{M}{r^*} \exp \zeta \\ &\quad + \frac{1}{\tau_0} (2\operatorname{sech}^2 \zeta - 1) + \left( \frac{3M}{r^*} + \frac{\tau_1}{2\sqrt{\tau_0} \varepsilon} \right) \operatorname{sech} \zeta (1 - \zeta \tanh \zeta), \\ \psi_1 &= \sqrt{\frac{\varepsilon}{\tau_0}} \left[ \left\{ 2A - \frac{4M}{r^*} + \frac{4N}{r^*} \arctan(\sinh \zeta) + \frac{8M}{r^*} \ln(\operatorname{sech} \zeta) - \left( \frac{6M}{r^*} + \frac{\tau_1}{\sqrt{\tau_0}} \right) \zeta \right\} \right. \\ &\quad \left. \times \operatorname{sech} \zeta + \frac{2M}{r^*} \exp \zeta - \left( \frac{N}{r^*} - \frac{2}{\tau_0} \right) \zeta - \left( \frac{4}{\tau_0} + \frac{2N}{r^*} \right) \tanh \zeta - B \right], \\ r_1 &= \sqrt{\frac{\varepsilon}{\tau_0}} [2N(\operatorname{sech} \zeta - \operatorname{sech} \Gamma) - 4M(\tanh \zeta - \tanh \Gamma) + 2M(\zeta - \Gamma)], \\ \varpi_1 &= -\sqrt{\frac{\varepsilon}{\tau_0}} r^* (\zeta - \Gamma), \end{aligned}$$

where  $\zeta \equiv \sqrt{\tau_0} \xi + \Gamma$ ,  $M = -\{\cos[\psi_0^* + 2 \arctan(\sinh \Gamma)]\}/2$ , and  $N = -\sin[\psi_0^* + 2 \arctan(\sinh \Gamma)]$ . Here,  $\Gamma$  and  $A$  are the constants of integration from the lowest- and first-order equations for  $H$ , respectively. They are determined using matching and jump conditions. The constant  $B$  is related to the value of the tangent angle  $\psi^*$  at the interface.

To obtain the order- $\mu$  term in  $h$  in the inner layer, it is necessary to consider the equation for  $H$  at order  $\mu^2$ :

$$\ddot{H}_2 - \left( \frac{\tau_0}{\varepsilon} - 6H_0^2 \right) H_2 = \frac{\tau_1}{\varepsilon} H_1 + \frac{\tau_2}{\varepsilon} H_0 + F(\xi), \tag{3.6}$$

where  $F(\xi)$  is implicitly given by

$$\begin{aligned} F(\xi) &= -\frac{2}{\varepsilon} \left( 3H_0 H_1^2 - 4H_0 H_1 \frac{\sin \psi_0}{r^*} + H_0 \frac{\sin^2 \psi_0}{(r^*)^2} \right) - \sqrt{\frac{\tau_0}{\varepsilon}} H_1 \frac{\cos \psi_0}{\varepsilon r^*} \\ &\quad - \left( 4H_0^2 \frac{\cos \psi_0}{r^*} - \sqrt{\frac{\tau_0}{\varepsilon}} \frac{\sin \psi_0}{r^*} \dot{H}_0 \right) \frac{\psi_1}{\varepsilon} + \left( 4H_0^2 \sin \psi_0 + \frac{\tau_0 \dot{H}_0}{\sqrt{\varepsilon}} \cos \psi_0 \right) \frac{r_1}{\varepsilon (r^*)^2}. \end{aligned}$$

The solution to (3.6) is given by

$$H_2 = C \operatorname{sech} \zeta \tanh \zeta + \frac{\tau_1}{\tau_0^2} \left( 1 - \frac{4}{3} \operatorname{sech}^2 \zeta \right) + g(\xi),$$

where  $C$  is an undetermined constant and  $g(\xi)$  is a complicated function that decays to zero as  $\xi$  goes to  $-\infty$ . The solutions of the  $H_1$  and  $H_2$  equations have one undetermined constant each, instead of two that are expected. When we impose boundedness of  $h$  as  $\xi$  goes to  $-\infty$ , and equate the coefficient of the exponentially growing terms collected together appearing in the solution to zero, one of the constants is determined. The



constants  $C$  and  $\tau_2$  cannot be determined from the order- $\mu$  analysis. They can be determined from the solutions at order  $\mu^2$ , which we do not attempt here. This leads to a small error in order- $\mu$  terms of  $h$ , as both  $\text{sech } \zeta \tanh \zeta$  and  $g(\xi)$  decay rapidly with  $\xi$ , and leaves the other variables unaffected. Note that  $H_2$  goes to  $\tau_1/\tau_0^2$ , its outer solution at order  $\mu$ , as  $\xi$  goes to  $-\infty$ .

3.3. Outer and inner layer for the (+) region

Following the same procedure, we obtain the outer layer for (2.6) and (2.7), corresponding to the (+) region, including terms of order  $\mu$ , as

$$h = -\frac{1}{\tau_0} + \mu \frac{\tau_1}{\tau_0^2}, \quad \psi = \pi - \frac{y}{\tau_0} + \mu \frac{\tau_1}{\tau_0^2} y, \quad r = \tau_0 \sin \frac{y}{\tau_0} + \mu \left\{ \tau_1 \sin \frac{y}{\tau_0} - \frac{\tau_1}{\tau_0} y \cos \frac{y}{\tau_0} \right\},$$

$$\varpi = \tau_0^2 \left( 1 - \cos \frac{y}{\tau_0} \right) - 1 + \mu \left[ 2\tau_0 \tau_1 \left( 1 - \cos \frac{y}{\tau_0} \right) - \tau_1 y \sin \frac{y}{\tau_0} \right],$$

and where  $y \equiv \hat{s} - s$ , in which  $\hat{s} \equiv \hat{s}_0 + \mu \hat{s}_1$  is the deformed arclength at the south pole.

The inner layer solution, up to order  $\mu$ , is

$$h = \frac{\sqrt{\tau_0}}{\mu} \text{sech } \eta + \left[ D + \frac{2T}{r^*} \arctan(\sinh \eta) + \frac{4P}{r^*} \ln(\text{sech } \eta) \right] \text{sech } \eta \tanh \eta$$

$$+ \frac{P}{r^*} \exp(-\eta) + \frac{1}{\tau_0} (2 \text{sech}^2 \eta - 1) + \left( \frac{\tau_1}{2\sqrt{\tau_0}} - \frac{3P}{r^*} \right) \text{sech } \eta (1 - \eta \tanh \eta)$$

$$+ \mu \left[ G \text{sech } \eta \tanh \eta + \frac{\tau_1}{\tau_0^2} \left( 1 - \frac{4}{3} \text{sech}^2 \eta \right) + f(\xi) \right],$$

$$\psi = \psi_0^* - 2[\arctan(\sinh \eta) - \arctan(\sinh \gamma)] + \frac{\mu}{\sqrt{\tau_0}} \left[ \left\{ 2D + \frac{4T}{r^*} \arctan(\sinh \eta) \right. \right.$$

$$+ \left. \frac{8P}{r^*} \ln(\text{sech } \eta) - \frac{4P}{r^*} + \left( \frac{6P}{r^*} - \frac{\tau_1}{\sqrt{\tau_0}} \right) \eta \right\} \text{sech } \eta + \frac{2P}{r^*} \exp(-\eta)$$

$$\left. - \left( \frac{T}{r^*} - \frac{2}{\tau_0} \right) \eta - \left( \frac{4}{\tau_0} + \frac{2T}{r^*} \right) \tanh \eta - E \right],$$

$$r = r^* + \frac{\mu}{\sqrt{\tau_0}} [2T (\text{sech } \eta - \text{sech } \gamma) - 4P (\tanh \eta - \tanh \gamma) + 2P(\eta - \gamma)],$$

$$\varpi = \varpi^* - \frac{\mu r^*}{\sqrt{\tau_0}} (\eta - \gamma),$$

where  $\eta = \sqrt{\tau_0} \xi + \gamma$ ,  $P = -\{\cos[\psi_0^* + 2 \arctan(\sinh \gamma)]\}/2$ , and  $T = -\sin[\psi_0^* + 2 \arctan(\sinh \gamma)]$ , and  $f(\xi)$  decays to zero as  $\xi$  goes to  $\infty$ . The constants  $\gamma$  and  $D$  are the constants of integration from the lowest- and first-order equations for  $H$ , respectively. They are solved using matching and jump conditions. The constant  $E$  is related to the value of the tangent angle  $\psi^*$  at the interface. The constant  $G$ , similar to the constant  $C$ , can be determined from the solutions at order  $\mu^2$ .

Note that  $\tau_0, \tau_1$  should be read as  $\tau_0^-, \tau_1^-$ , respectively for (-) region and  $\tau_0^+, \tau_1^+$ , respectively for (+) region and the same for  $h, \psi, r$ , and  $\varpi$ .

4. Jump conditions and asymptotic matching for the boundary layer

We have, so far, determined solutions for the inner and outer layers that are valid separately in the boundary layer and away from the boundary layer, respectively.

They involve constants and parameters that are yet to be determined. We solve for these using the equations obtained from asymptotic matching of the outer and the inner layers, and the jump conditions at the interface. In doing so, we also obtain a composite solution that is uniformly valid over the entire region. For asymptotic matching, we make the inner and outer solutions agree in an intermediate region (Hinch 1991; Bender & Orszag 1999). To obtain expressions for the inner layer in an intermediate region, we let  $\xi$  go to  $-\infty$  in the  $(-)$  region and to  $\infty$  in the  $(+)$  region. We then retain terms of order one, order  $\mu$ , and order  $\mu\xi$ . After the substitutions  $s = s^* + \mu\xi$  and  $s^* = s_0^* + \mu s_1^*$  the outer layer solutions are expanded in powers of  $\mu$ . Corresponding order-one, order- $\mu$ , and order- $\mu\xi$  terms resulting from the inner and outer solutions are equated after taking the limits. The matching of  $h$  is identically satisfied, because of the restriction of no oscillation and the boundedness imposed on  $H_0$ ,  $H_1$ , and  $H_2$ . At the interface the boundary radius  $r^*$  is specified, the parameters  $\psi^*$  and  $\sigma$  are expanded as

$$\psi^* = \psi_0^* + \mu\psi_1^*, \quad \sigma = \sigma_0 + \mu\sigma_1,$$

and the jump conditions are satisfied at the order one and order  $\mu$ . It would be truer to the physics to treat the line tension  $\sigma$  as a known quantity and the boundary radius  $r^*$  as an unknown to be determined. In that case, the boundary radius should be expanded as  $r^* = r_0^* + \mu r_1^*$  and  $\sigma$  should be regarded as an input.

4.1. *Jump conditions and asymptotic matching for the boundary layer at the lowest order*

The solution of the matching and jump conditions at the lowest order indicates that only the tangent angle at the interface is influenced by the bending stiffness. All other quantities are determined by the zero-bending solution discussed in Allain & BenAmar (2006). However, in Allain & BenAmar (2006) the inner and outer layer solutions of the full system of equations and their matching was not attempted. Consequently, the geometric quantities such as radii of the outer spheres, and the tangent angles at the intersection of the two spheres are specified as inputs in their analysis. Here, we solve the matching and jump conditions analytically. Then, in addition to the osmotic pressure, also employed as input by Allain & BenAmar (2006), only the area fraction of the disordered phase  $\chi^+$  and the boundary radius  $r^*$  need to be specified. These two quantities can be obtained from vesicle shape tracing (Baumgart *et al.* 2005; Das 2007).

Boundary layer matching of  $\psi$ ,  $r$ , and  $\varpi$ , in the  $(-)$  and  $(+)$  region at the lowest order gives

$$r^* = \tau_0^- \sin \frac{s_0^*}{\tau_0^-}, \quad (\tau_0^-)^2 \left( \cos \frac{s_0^*}{\tau_0^-} - 1 \right) + 2 = 2\chi^+, \tag{4.1}$$

$$r^* = \tau_0^+ \sin \frac{\hat{s}_0 - s_0^*}{\tau_0^+}, \quad (\tau_0^+)^2 \left( 1 - \cos \frac{\hat{s}_0 - s_0^*}{\tau_0^+} \right) = 2\chi^+, \tag{4.2}$$

$$\arctan(\sinh \Gamma) = -\frac{\pi}{2} - \frac{\psi_0^*}{2} + \frac{s_0^*}{2\tau_0^-}, \quad \arctan(\sinh \Upsilon) = \pi - \frac{\psi_0^*}{2} - \frac{\hat{s}_0 - s_0^*}{2\tau_0^+}. \tag{4.3}$$

The jump conditions, at this order, given by (2.10) to (2.12), become

$$H_0^+ - \varepsilon H_0^- = 0,$$

$$\sqrt{\tau_0^+} \frac{dH_0^+}{d\eta} - \sqrt{\varepsilon \tau_0^-} \frac{dH_0^-}{d\xi} + \sigma_0 \frac{\sin \psi_0^*}{r^*} = 0,$$

$$\frac{1}{2}(\tau_0^+ - \tau_0^-) - [(H_0^+)^2 - \varepsilon(H_0^-)^2] - \sigma_0 \frac{\cos \psi_0^*}{r^*} = 0.$$

The explicit forms of the above jump conditions in terms of the unknown parameters are

$$\sqrt{\tau_0^+} \operatorname{sech} \Upsilon - \sqrt{\varepsilon \tau_0^-} \operatorname{sech} \Gamma = 0, \tag{4.4}$$

$$\tau_0^+ \operatorname{sech} \Upsilon \tanh \Upsilon - \tau_0^- \operatorname{sech} \Gamma \tanh \Gamma - \sigma_0 \frac{\sin \psi_0^*}{r^*} = 0, \tag{4.5}$$

$$\frac{1}{2}(\tau_0^+ - \tau_0^-) - (\tau_0^+ \operatorname{sech}^2 \Upsilon - \tau_0^- \operatorname{sech}^2 \Gamma) - \sigma_0 \frac{\cos \psi_0^*}{r^*} = 0. \tag{4.6}$$

The solution of (4.1) and (4.2) is

$$\tau_0^- = \frac{2(1 - \chi^+)}{\sqrt{4(1 - \chi^+) - (r^*)^2}}, \quad \tau_0^+ = \frac{2\chi^+}{\sqrt{4\chi^+ - (r^*)^2}}, \tag{4.7}$$

$$s_0^* = \tau_0^- \arcsin \left( \frac{r^* \sqrt{4(1 - \chi^+) - (r^*)^2}}{2(1 - \chi^+)} \right), \quad \hat{s}_0 = s_0^* + \tau_0^+ \arcsin \left( \frac{\sqrt{4\chi^+ - (r^*)^2}}{2\chi^+} \right). \tag{4.8}$$

From the lowest-order outer solution,

$$\sigma_0 = \frac{r^*}{2} \left( \frac{2\chi^+ - (r^*)^2}{\sqrt{4\chi^+ - (r^*)^2}} + \frac{2(1 - \chi^+) - (r^*)^2}{\sqrt{4(1 - \chi^+) - (r^*)^2}} \right). \tag{4.9}$$

Equations (4.3) and (4.4) give

$$\left( \varepsilon \tau_0^- \cos \frac{s_0^*}{\tau_0^-} + \tau_0^+ \cos \frac{\hat{s}_0 - s_0^*}{\tau_0^+} \right) \cos \psi_0^* + r^* (\varepsilon - 1) \sin \psi_0^* = \varepsilon \tau_0^- - \tau_0^+. \tag{4.10}$$

This equation can be solved in closed form. A unique solution is obtained when we impose the condition that  $0 \leq \psi_0^* \leq \pi$ . Finally, it can be verified that (4.5) and (4.6) are automatically satisfied, using  $\sigma_0$  given by (4.9).

When  $\varepsilon = 1$  and  $\chi^+ = 1/2$ , the solution to (4.10) is  $\psi_0^* = \pi/2$  and the interface is at the neck. When this symmetry is broken by taking  $\varepsilon$  different from unity and/or  $\chi^+$  different from  $1/2$ , this is not the case. We will see in the next section that a difference in Gaussian curvature stiffnesses  $\Delta$  also influences the position of the interface relative to the neck.

#### 4.2. Jump conditions and asymptotic matching for the boundary layer at order $\mu$

In this section, we obtain and solve the matching and jump conditions at order  $\mu$ . The jump in bending moment at this order involves the measure  $\Delta$  of the difference in Gaussian curvature resistances. The value of the tangent angle at the interface and, consequently, the location of the interface with respect to the neck are influenced by  $\Delta$  (Jülicher & Lipowsky 1996; Baumgart *et al.* 2005). This is not captured by the lowest-order solution of Allain & Ben Amar (2006).

Asymptotic matching of  $r$  and  $\varpi$  for the two regions gives

$$\tau_1^- \left[ 2 \tau_0^- \left( \cos \frac{s_0^*}{\tau_0^-} - 1 \right) + \frac{s_0^*}{\tau_0^-} r^* \right] - r^* s_1^* = 0, \tag{4.11}$$

$$\tau_1^- \left( \frac{r^*}{\tau_0^-} - \frac{s_0^*}{\tau_0^-} \cos \frac{s_0^*}{\tau_0^-} \right) + \cos \frac{s_0^*}{\tau_0^-} s_1^* = \Lambda_1, \tag{4.12}$$

$$\tau_1^+ \left[ 2\tau_0^+ \left( \cos \frac{\widehat{s}_0 - s_0^*}{\tau_0^+} - 1 \right) + \frac{\widehat{s}_0 - s_0^*}{\tau_0^+} r^* \right] - r^* (\widehat{s}_1 - s_1^*) = 0, \quad (4.13)$$

$$\tau_1^+ \left( \frac{r^*}{\tau_0^+} - \frac{\widehat{s}_0 - s_0^*}{\tau_0^+} \cos \frac{\widehat{s}_0 - s_0^*}{\tau_0^+} \right) + \cos \frac{\widehat{s}_0 - s_0^*}{\tau_0^+} (\widehat{s}_1 - s_1^*) = \Lambda_2. \quad (4.14)$$

The expressions for  $\Lambda_1$  and  $\Lambda_2$  are provided in Appendix C. Solving (4.11) to (4.14),

$$\tau_1^- = (r^* \Lambda_1) / \left[ \tau_0^- \left( 1 - \cos \frac{s_0^*}{\tau_0^-} \right)^2 \right], \quad \tau_1^+ = (r^* \Lambda_2) / \left[ \tau_0^+ \left( 1 - \cos \frac{\widehat{s}_0 - s_0^*}{\tau_0^+} \right)^2 \right], \quad (4.15)$$

$$s_1^* = \Lambda_1 \left[ 2\tau_0^- \left( \cos \frac{s_0^*}{\tau_0^-} - 1 \right) + \frac{s_0^*}{\tau_0^-} r^* \right] / \left[ \tau_0^- \left( 1 - \cos \frac{s_0^*}{\tau_0^-} \right)^2 \right], \quad (4.16)$$

$$\widehat{s}_1 = s_1^* + \Lambda_2 \left[ 2\tau_0^+ \left( \cos \frac{\widehat{s}_0 - s_0^*}{\tau_0^+} - 1 \right) + \frac{\widehat{s}_0 - s_0^*}{\tau_0^+} r^* \right] / \left[ \tau_0^+ \left( 1 - \cos \frac{\widehat{s}_0 - s_0^*}{\tau_0^+} \right)^2 \right]. \quad (4.17)$$

Asymptotic matching of  $\psi_1$  for the two regions gives

$$\psi_1^* - \left( 2\sqrt{\frac{\varepsilon}{\tau_0^-}} \operatorname{sech} \Gamma \right) A = \Lambda_3, \quad \psi_1^* - \left( 2\sqrt{\frac{1}{\tau_0^+}} \operatorname{sech} \Upsilon \right) D = \Lambda_4. \quad (4.18)$$

By satisfying the jump conditions at order  $\mu$ ,

$$H_1^+ - \varepsilon H_1^- - \Delta \frac{\sin \psi_0^*}{r^*} = 0, \quad (4.19)$$

$$\frac{\tau_1^+}{2} - \frac{\tau_1^-}{2} - 2(H_0^+ H_1^+ - \varepsilon H_0^- H_1^-) + \sigma_0 \frac{\sin \psi_0^*}{r^*} \psi_1^* - \sigma_1 \frac{\cos \psi_0^*}{r^*} = 0, \quad (4.20)$$

$$\sqrt{\tau_0^+} \frac{dH_1^+}{d\eta} - \sqrt{\varepsilon \tau_0^-} \frac{dH_1^-}{d\zeta} + \sigma_0 \left( \frac{\cos \psi_0^*}{r^*} \psi_1^* \right) + \sigma_1 \frac{\sin \psi_0^*}{r^*} = 0. \quad (4.21)$$

Rewriting (4.19) and (4.20),

$$(\operatorname{sech} \Upsilon \tanh \Upsilon) D - (\varepsilon \operatorname{sech} \Gamma \tanh \Gamma) A = \Lambda_5, \quad (4.22)$$

$$(\sqrt{\tau_0^+} \operatorname{sech}^2 \Upsilon \tanh \Upsilon) D - (\sqrt{\varepsilon \tau_0^-} \operatorname{sech}^2 \Gamma \tanh \Gamma) A - \sigma_0 \frac{\sin \psi_0^*}{2r^*} \psi_1^* + \frac{\cos \psi_0^*}{2r^*} \sigma_1 = \frac{\Lambda_6}{2}. \quad (4.23)$$

The expressions for  $\Lambda_3$  to  $\Lambda_6$  are provided in Appendix C. Only  $\Lambda_5$  contains the measure of Gaussian curvature stiffness  $\Delta$ .

Upon solving (4.18) and (4.22) for  $\psi_1^*$ ,  $A$ , and  $D$  and simplifying the resulting expressions we obtain

$$\psi_1^* = \Omega_{11} \Lambda_3 + \Omega_{12} \Lambda_4 + \Omega_{13} \Lambda_5, \quad (4.24)$$

$$A = \Omega_{21} (\Lambda_4 - \Lambda_3) + \Omega_{22} \Lambda_5, \quad D = \Omega_{31} (\Lambda_4 - \Lambda_3) + \Omega_{32} \Lambda_5. \quad (4.25)$$

Subsequently, we solve for  $\sigma_1$  using (4.23) when  $\psi_0^*$  is not equal to  $\pi/2$  and obtain

$$\sigma_1 = -\frac{r^*}{\cos \psi_0^*} (\Omega_{41} \Lambda_3 + \Omega_{42} \Lambda_4 - \Lambda_6). \quad (4.26)$$

When  $\psi_0^*$  is equal to  $\pi/2$ ,  $\sigma_1$  can be solved using (4.21). The coefficients  $\Omega_{ij}$  are given in Appendix D.

The solution at order  $\mu$ , given by (4.15) to (4.17) and (4.24) to (4.26), is one of the main contributions of our paper. Note, from (4.24) and (4.25), that  $\Delta$  influences the values of  $\psi_1^*$ ,  $A$ , and  $D$ . Moreover, (4.26) shows that  $\Lambda_5$  does not appear in the solution for  $\sigma_1$ . This implies that the line tension is not influenced by the Gaussian curvature stiffness. Finally, we provide the composite solutions that are uniformly valid for the entire vesicle in Appendix E.

## 5. Discussion

### 5.1. A simple situation

Here we consider the situation when both the phases have same mean curvature bending stiffness and area fraction. In this case  $\varepsilon = 1$  and  $\chi^+ = 1/2$ . The boundary radius  $r^*$ , although an order-one quantity, is always smaller than unity. Consequently, we express the results for this simple situation in powers of  $r^*$ . We keep terms up to and including  $(r^*)^4$ . Quantities at the lowest order from (4.7) to (4.10) are

$$\begin{aligned} \tau_0^- = \tau_0^+ &= \frac{1}{\sqrt{2 - (r^*)^2}} \approx \frac{1}{\sqrt{2}} \left[ 1 + \frac{1}{4} (r^*)^2 + \frac{3}{32} (r^*)^4 \right], \\ s_0^* &= \frac{\hat{s}_1}{2} \approx \frac{\pi}{\sqrt{2}} - r^* + \frac{\pi}{4\sqrt{2}} (r^*)^2 - \frac{1}{3} (r^*)^3 + \frac{3\pi}{32\sqrt{2}} (r^*)^4, \\ \sigma_0 &= \frac{r^* - (r^*)^3}{\sqrt{2 - (r^*)^2}} \approx \frac{r^*}{\sqrt{2}} \left[ 1 - \frac{3}{4} (r^*)^2 - \frac{1}{32} (r^*)^4 \right], \quad \psi_0^* = \frac{\pi}{2}, \\ \Gamma &= -\Upsilon \approx -\ln(1 + \sqrt{2}) - r^* - \frac{\sqrt{2}}{4} (r^*)^2 - \frac{1}{3} (r^*)^3 - \frac{5\sqrt{2}}{32} (r^*)^4. \end{aligned}$$

At order  $\mu$ ,

$$\Lambda_1 = \Lambda_2, \quad \Lambda_3 = -\Lambda_4, \quad \Lambda_5 = \frac{\Delta}{r^*}, \quad \Lambda_6 = 0.$$

Upon evaluating the expressions for the  $\Lambda_i$  and  $\Omega_{ij}$  given in Appendices C and D, respectively,

$$\begin{aligned} \tau_1^- = \tau_1^+ &\approx -0.24629 r^* - 0.42045 (r^*)^2 + 0.53831 (r^*)^3 - 0.26278 (r^*)^4, \\ s_1^* &= \frac{\hat{s}_1}{2} \approx 0.69662 + 0.41545 r^* - 2.66930 (r^*)^2 + 2.73171 (r^*)^3 - 2.12520 (r^*)^4, \\ \psi_1^* &\approx \frac{\Delta}{r^*} [1.68179 - 1.18921 r^* + 1.05112 (r^*)^2 - 1.04056 (r^*)^3 + 1.01170 (r^*)^4]. \end{aligned} \tag{5.1}$$

Because  $\psi^* = \pi/2$ , using (4.21) we obtain

$$\sigma_1 \approx -0.98517 + 3.36358 r^* - 2.15325 (r^*)^2 + 0.84090 (r^*)^3 - 0.93567 (r^*)^4.$$

All the coefficients in the above expansions are correct up to four decimal places. Because the error in the above expansions is of the order  $(r^*)^5 \approx 10^{-5}$ , the coefficient of  $(r^*)^i$  in each expansion, where  $i$  is between 0 and 4, need only be correct up to  $(4 - i)$  decimal places.

Equation (5.1) explicitly determines the dependence of the tangent angle at the interface and the shifting of the phase boundary away from the neck on the difference in the Gaussian curvature stiffnesses between the domains. This was

observed previously for budding of a vesicle by Jülicher & Lipowsky (1996). In experimental images of vesicles with two fluid domains, it is also observed that the phase boundary is not at the neck (Baumgart *et al.* 2005). However, in experimental situations, the shifting of the phase boundary away from the neck is a combined effect of the different mean curvature bending stiffnesses ( $\varepsilon \neq 1$ ), different Gaussian curvature bending stiffnesses ( $\Delta \neq 0$ ), and unequal area fractions ( $\chi^+ \neq 1/2$ ). In this situation, the expressions given by (4.7) to (4.10), (4.15) to (4.17), and (4.24) to (4.26) need to be evaluated numerically.

### 5.2. General case: comparison between analytical and numerical solutions for experimentally relevant situation

We now compare our boundary layer results with the results obtained from numerical integration of the shape equations (2.2) to (2.5) along with the jump conditions (2.8) to (2.10) and the boundary conditions (2.13) and (2.14) for parameter values that were employed to analyse experimental shapes in Baumgart *et al.* (2005).

The geometric description of the experimental vesicle that was analysed (figure 2A of Baumgart *et al.* (2005)) are:  $L_d$  phase area fraction  $\chi^+ \approx 0.56$ ,  $r^* \approx 0.34$ . Corresponding to  $\chi^+ = 0.56$ , using (2.15), we obtain  $S^* = 1.45$ , or  $\varpi^* = 0.12$ . The best-fit result to this experimental shape using numerical integration gave  $\varepsilon = 5$ ,  $\Delta = 3.6$ , a pressure  $\hat{p} = -333.11$  (outer excess), and a line tension  $\hat{\sigma} = 73.45$ . In the analytical solution, we employ  $\mu = 0.055$ , which corresponds to  $p = 333.11$  (inner excess), and obtain  $\sigma = 0.21$ , or equivalently,  $\hat{\sigma} = \sigma p = 71.15$ . A comparison between tangent angles of the numerical solution and the boundary layer solution in the neck region is shown in figure 2(a). The analytical expressions for the tangent angle, for the (−) and the (+) regions, are  $\psi^-(s) = \psi_0^-(s) + \mu \psi_1^-(s)$  and  $\psi^+(s) = \psi_0^+(s) + \mu \psi_1^+(s)$ , respectively, where  $\psi_0^-(s)$ ,  $\psi_1^-(s)$ ,  $\psi_0^+(s)$ ,  $\psi_1^+(s)$  are given in Appendix E.

Using the mechanical parameters  $\varepsilon = 5$  and  $\Delta = 3.6$ , numerical shapes that correspond to experimental shapes 2D and 2G of Baumgart *et al.* (2005) were obtained. We compare numerical and analytical solutions for the tangent angle in the neck region for those cases in figures 2(b) and 2(c). In figure 2(b), the input parameters to the analytical solution are  $\chi^+ \approx 0.18$ ,  $r^* \approx 0.24$ , and  $\mu = 0.051$  (or  $p = 387.62$ ). The values of the line tension obtained from boundary layer analysis and numerical integration, in this case, are  $\hat{\sigma} = 52.75$  and  $\hat{\sigma} = 54.27$ , respectively. In figure 2(c), the input parameters are  $\chi^+ \approx 0.89$ ,  $r^* \approx 0.52$ , and  $\mu = 0.022$  (or  $p = 2125.78$ ). The line tension calculated from boundary layer analysis and numerical integration are  $\hat{\sigma} = 405.91$  and  $\hat{\sigma} = 423.73$ , respectively. In all of these, we observe good agreement. We have also compared analytical and numerical solutions for a variety of other parameter values and obtained good matches. They are not presented here.

The excellent agreement between numerical and analytical solutions suggest that the approximate expression for the tangent angle near the interface can be used to extract the difference in Gaussian curvature stiffnesses  $\Delta$  and line tension  $\sigma$  from experimental vesicles data. Use of the analytical expression will eliminate the need for the repeated generation of numerical solutions in the estimation of the material parameters (Baumgart *et al.* 2005). The higher-order boundary layer analysis, presented here, with the incorporation of the influence of  $\Delta$ , will play a key role in this determination. Analytical expressions for the tangent angle for the (−) and (+) regions, obtained via quadratic polynomials in the arclength around the interface, have been used for the estimation of parameters by Semrau *et al.* (2007). However, they considered the derivative of the tangent angle across the interface to be continuous,

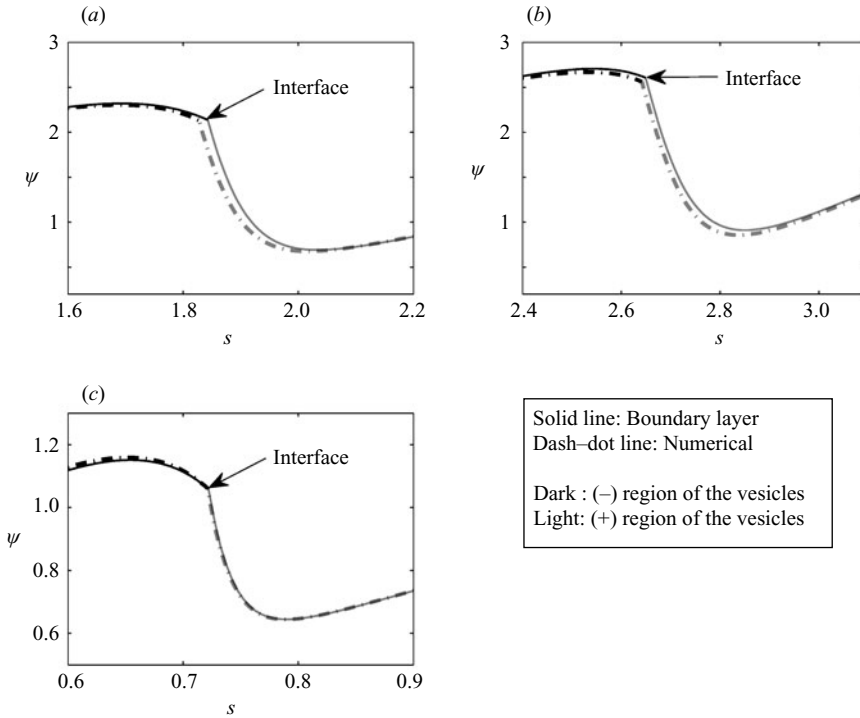


FIGURE 2. Comparison between the analytical and numerical solutions of the tangent angle in the neck region for  $\varepsilon = 5$  and  $\Delta = 3.6$ . The other input parameters ( $\chi^+$ ,  $r^*$ ,  $\mu$ ) are: (a) (0.56, 0.34, 0.055), (b) (0.18, 0.24, 0.051), and (c) (0.89, 0.52, 0.022). The tangent angle at the interface, in all cases, is different from  $\pi/2$ . The geometric quantities used as inputs for solutions in (a), (b), and (c) correspond to the experimental vesicles shown in figures 2A, 2D, and 2G of Baumgart *et al.* (2005), respectively.

which is not always the case and restricts the applicability of their technique. The expressions for tangent angle that we obtain here, by solving the shape equations, are not restricted by any such condition and exhibit proper physical behaviour of the membrane and can determine elastic parameters more accurately using experimental data. We will address this issue in future work.

### 5.3. Influence of $\varepsilon$ and $\Delta$ on the details of a non-symmetric shape

In a non-symmetric situation, at the lowest order, the expressions given by (4.7) to (4.10) indicate that  $s_0^*$ ,  $\hat{s}_0$ ,  $\tau_0^-$ ,  $\tau_0^+$ , and  $\sigma_0$  are not influenced by  $\varepsilon$  or  $\Delta$ , which means that they are determined by the outer solution alone. The tangent angle  $\psi_0^*$  at the interface is influenced by  $\varepsilon$ . When  $\chi^+ = 1/2$  and  $\varepsilon$  is close to unity,  $\psi_0^*$  is approximately given by

$$\psi_0^* \approx \frac{\pi}{2} - \left( \frac{\varepsilon - 1}{\varepsilon + 1} \right) \frac{1}{1 - r^*},$$

the neck forms at a location away from the interface, and the neck radius is smaller than the boundary radius  $r^*$ . At order  $\mu$ , the values of  $s_1^*$ ,  $\hat{s}_1$ ,  $\tau_1^-$ ,  $\tau_1^+$ ,  $\psi_1^*$ , and  $\sigma_1$  are influenced by  $\varepsilon$ , but not significantly. Interestingly,  $\Delta$  has an influence only on  $\psi_1^*$ .

## 6. Conclusions

In this work, we present approximate analytical solutions of the shape equations for giant unilamellar vesicles with fluid phase coexistence using a boundary layer analysis up to and including terms of first order. Our analytical solution reduces the number of measurements needed as inputs for the existing lowest-order analysis of Allain & Ben Amar (2006). The boundary layer calculation agrees well with the numerical solution for a variety of parameter values. Also, using the best-fit parameter values of Baumgart *et al.* (2005), we show that the shapes obtained from the boundary layer analysis match well with the experimental shapes. Our higher-order analysis incorporates the influence of Gaussian curvature not considered in earlier analytical work. The expression that we obtain here for the tangent angle in the neck region can be used to efficiently and accurately estimate elastic parameters, such as the line tension and Gaussian curvature stiffness, from experimental data.

We thank Anindya Chatterjee for his helpful comments on an earlier draft of the manuscript. We are also grateful to Tobias Baumgart for sustaining our interest in the subject and for many helpful discussions.

## Appendix A. Lowest-order outer layer for the (–) region

The equations at the lowest order are

$$h_0 = -\frac{1}{\tau_0}, \quad \psi'_0 = \frac{2}{\tau_0} - \frac{\sin \psi_0}{r_0}, \quad r'_0 = \cos \psi_0, \quad \varpi'_0 = -r_0, \quad (\text{A } 1)$$

with the boundary conditions

$$\psi_0(0) = 0, \quad r_0(0) = 0, \quad \varpi_0(0) = 1.$$

The solution at this order is given by

$$\psi_0 = \frac{s}{\tau_0}, \quad r_0 = \tau_0 \sin \frac{s}{\tau_0}, \quad \varpi_0 = \tau_0^2 \left( \cos \frac{s}{\tau_0} - 1 \right) + 1. \quad (\text{A } 2)$$

The outer solution, at this order, is a spherical cap of radius  $\tau_0$ .

## Appendix B. Lowest-order inner layer for the (–) region

At the lowest order the equations (from (3.4) and (3.5)) in the inner layer are

$$\ddot{H}_0 - \frac{\tau_0}{\varepsilon} H_0 + 2H_0^3 = 0, \quad \dot{\psi}_0 = -2H_0, \quad \dot{r}_0 = 0, \quad \dot{\varpi}_0 = 0. \quad (\text{B } 1)$$

At this order, the solution for  $H_0$  is given in terms of the Jacobi elliptic cosine function:

$$H_0 = C \operatorname{cn}(A \xi + \Gamma, k), \quad (\text{B } 2)$$

where  $A \equiv \sqrt{2C^2 - \tau_0/\varepsilon}$  and  $k \equiv C/\sqrt{2C^2 - \tau_0/\varepsilon}$ . In the experimental vesicles (Baumgart *et al.* 2003, 2005) and in the numerical solutions (Baumgart *et al.* 2005), it is observed that  $h$  decays monotonically from a maximum value at the phase boundary to the outer limiting value. This behaviour is obtained only if we take  $k = 1$  in (B 2) to obtain

$$H_0 = \sqrt{\frac{\tau_0}{\varepsilon}} \operatorname{sech} \zeta, \quad \text{where} \quad \zeta \equiv \sqrt{\frac{\tau_0}{\varepsilon}} \xi + \Gamma.$$



This reduces the number of undetermined constants in the solution from two to one. Using the above, the solutions for  $\psi_0$ ,  $r_0$ , and  $\varpi_0$  are

$$\psi_0 = \psi_0^* - 2[\arctan(\sinh \zeta) - \arctan(\sinh \Gamma)], \quad r_0 = r^*, \quad \varpi_0 = \varpi^* = \cos S^*,$$

where, at this order,  $\psi_0^*$  is the tangent angle and  $S^*$  is the value of the undeformed arclength at the interface measured from the north pole. This solution for the tangent angle is equivalent to that of Allain & Ben Amar (2006).

### Appendix C. Expressions for $\Lambda_1$ to $\Lambda_6$

$$\begin{aligned} \Lambda_1 &= \sqrt{\frac{\varepsilon}{\tau_0^-}} \left[ 2 \cos \frac{s_0^*}{\tau_0} (1 + \tanh \Gamma) - \frac{2r^*}{\tau_0^-} \operatorname{sech} \Gamma \right], \\ \Lambda_2 &= \sqrt{\frac{1}{\tau_0^+}} \left[ 2 \cos \frac{\widehat{s}_0 - s_0^*}{\tau_0^+} (1 - \tanh \Upsilon) - \frac{2r^*}{\tau_0^+} \operatorname{sech} \Upsilon \right], \\ \Lambda_3 &= \frac{s_1^*}{\tau_0} - \tau_1^- \left( \frac{s_0^*}{(\tau_0^-)^2} + \frac{\sqrt{\varepsilon}}{\tau_0} \Gamma \operatorname{sech} \Gamma \right) + \sqrt{\frac{\varepsilon}{\tau_0^-}} \left\{ \left[ \cos \frac{s_0^*}{\tau_0} \left( \frac{4}{r^*} \ln(\operatorname{sech} \Gamma) - \frac{3}{r^*} \Gamma - \frac{2}{r^*} \right) \right. \right. \\ &\quad \left. \left. + \frac{4}{\tau_0} \arctan(\sinh \Gamma) \right] \operatorname{sech} \Gamma + \frac{1}{r^*} \cos \frac{s_0^*}{\tau_0} \exp(\Gamma) - \frac{6}{\tau_0^-} (1 + \tanh \Gamma) \right\}, \\ \Lambda_4 &= -\frac{\widehat{s}_1 - s_1^*}{\tau_0^+} + \tau_1^+ \left( \frac{\widehat{s}_0 - s_0^*}{(\tau_0^+)^2} - \frac{\Upsilon}{\tau_0^+} \operatorname{sech} \Upsilon \right) + \sqrt{\frac{1}{\tau_0^+}} \left\{ \left[ \frac{4}{\tau_0^+} \arctan(\sinh \Upsilon) \right. \right. \\ &\quad \left. \left. + \cos \frac{\widehat{s}_0 - s_0^*}{\tau_0^+} \left( -\frac{3}{r^*} \Upsilon + \frac{2}{r^*} - \frac{4}{r^*} \ln(\operatorname{sech} \Upsilon) \right) \right] \operatorname{sech} \Upsilon \right. \\ &\quad \left. - \frac{1}{r^*} \cos \frac{\widehat{s}_0 - s_0^*}{\tau_0^+} \exp(-\Upsilon) + \frac{6}{\tau_0^+} (1 - \tanh \Upsilon) \right\}, \\ \Lambda_5 &= \Delta \frac{\sin \psi_0^*}{r^*} + (\varepsilon \operatorname{sech} \Gamma \tanh \Gamma) \left[ \frac{2}{\tau_0^-} \arctan(\sinh \Gamma) + \frac{2}{r^*} \cos \frac{s_0^*}{\tau_0} \ln(\operatorname{sech} \Gamma) \right] \\ &\quad - \frac{\varepsilon}{2r^*} \cos \frac{s_0^*}{\tau_0} e^\Gamma + \frac{\varepsilon}{\tau_0^-} (2 \operatorname{sech}^2 \Gamma - 1) + \frac{\varepsilon}{2} \left( \frac{3}{r^*} \cos \frac{s_0^*}{\tau_0} + \frac{\tau_1^-}{\sqrt{\varepsilon \tau_0^-}} \right) \operatorname{sech} \Gamma (1 - \Gamma \tanh \Gamma) \\ &\quad - (\operatorname{sech} \Upsilon \tanh \Upsilon) \left[ \frac{2}{\tau_0^+} \arctan(\sinh \Upsilon) - \frac{2}{r^*} \cos \frac{\widehat{s}_0 - s_0^*}{\tau_0^+} \ln(\operatorname{sech} \Upsilon) \right] \\ &\quad + \frac{1}{2r^*} \cos \frac{\widehat{s}_0 - s_0^*}{\tau_0^+} e^{-\Upsilon} - \frac{1}{\tau_0^+} (2 \operatorname{sech}^2 \Upsilon - 1) \\ &\quad - \frac{1}{2} \left( \frac{3}{r^*} \cos \frac{\widehat{s}_0 - s_0^*}{\tau_0^+} + \frac{\tau_1^+}{\sqrt{\tau_0^+}} \right) \operatorname{sech} \Upsilon (1 - \Upsilon \tanh \Upsilon), \\ \Lambda_6 &= \frac{\tau_1^+ - \tau_1^-}{2} + (\sqrt{\varepsilon \tau_0^-} \operatorname{sech}^2 \Gamma \tanh \Gamma) \left[ \frac{2}{\tau_0^-} \arctan(\sinh \Gamma) + \frac{2}{r^*} \cos \frac{s_0^*}{\tau_0} \ln(\operatorname{sech} \Gamma) \right] \\ &\quad + \sqrt{\frac{\varepsilon}{\tau_0^-}} \operatorname{sech} \Gamma (2 \operatorname{sech}^2 \Gamma - 1) + \frac{\sqrt{\varepsilon \tau_0^-}}{2} \left( \frac{3}{r^*} \cos \frac{s_0^*}{\tau_0} + \frac{\tau_1^-}{\sqrt{\varepsilon \tau_0^-}} \right) \end{aligned}$$

$$\begin{aligned} & \times \operatorname{sech}^2 \Gamma (1 - \Gamma \tanh \Gamma) - \frac{\sqrt{\varepsilon \tau_0^-}}{2r^*} \cos \frac{s_0^*}{\tau_0^-} \operatorname{sech} \Gamma e^\Gamma + \frac{\sqrt{\tau_0^+}}{2r^*} \cos \frac{\widehat{s}_0 - s_0^*}{\tau_0^+} \operatorname{sech} \Upsilon e^{-\Upsilon} \\ & - \frac{1}{\sqrt{\tau_0^+}} \operatorname{sech} \Upsilon (2 \operatorname{sech}^2 \Upsilon - 1) - (\sqrt{\tau_0^+} \operatorname{sech}^2 \Upsilon \tanh \Upsilon) \left[ \frac{2}{\tau_0^+} \arctan(\sinh \Upsilon) \right. \\ & \left. - \frac{2}{r^*} \cos \frac{\widehat{s}_0 - s_0^*}{\tau_0^+} \ln(\operatorname{sech} \Upsilon) \right] - \frac{\sqrt{\tau_0^+}}{2} \left( \frac{3}{r^*} \cos \frac{\widehat{s}_0 - s_0^*}{\tau_0^+} + \frac{\tau_1^+}{\sqrt{\tau_0^+}} \right) \\ & \times \operatorname{sech}^2 \Upsilon (1 - \Upsilon \tanh \Upsilon). \end{aligned}$$

**Appendix D. Expressions for  $\Omega_{11}$  to  $\Omega_{42}$**

$$\begin{aligned} \Omega_{11} &= -\frac{2\varepsilon}{\Omega \sqrt{\tau_0^+}} (\operatorname{sech} \Gamma \tanh \Gamma \operatorname{sech} \Upsilon), & \Omega_{12} &= \frac{2}{\Omega} \sqrt{\frac{\varepsilon}{\tau_0^-}} (\operatorname{sech} \Gamma \operatorname{sech} \Upsilon \tanh \Upsilon), \\ \Omega_{13} &= \frac{4}{\Omega} \sqrt{\frac{\varepsilon}{\tau_0^- \tau_0^+}} (\operatorname{sech} \Gamma \operatorname{sech} \Upsilon), & \Omega_{21} &= \frac{1}{\Omega} (\operatorname{sech} \Upsilon \tanh \Upsilon), & \Omega_{22} &= \frac{2}{\Omega \sqrt{\tau_0^+}} \operatorname{sech} \Upsilon, \\ \Omega_{31} &= \frac{\varepsilon}{\Omega} (\operatorname{sech} \Gamma \tanh \Gamma), & \Omega_{32} &= \frac{2}{\Omega} \sqrt{\frac{\varepsilon}{\tau_0^-}} \operatorname{sech} \Gamma, \\ \Omega_{41} &= \sqrt{\frac{\tau_0^-}{\varepsilon}} \tanh \Gamma \operatorname{sech} \Upsilon, & \Omega_{42} &= -\tau_0^+ (\operatorname{sech} \Upsilon \tanh \Upsilon), \end{aligned}$$

where

$$\Omega = \frac{2\varepsilon \operatorname{sech}^2 \Gamma}{\tau_0^+} \left[ \sqrt{\tau_0^+} \tanh \Upsilon - \sqrt{\varepsilon \tau_0^-} \tanh \Gamma \right].$$

**Appendix E. Composite solution**

Composite solutions, that are valid for the entire region, are obtained using the relation

$$\text{Composite solution} = \text{Inner} + \text{Outer} - \text{Matching}.$$

The composite solutions at lowest order for the (−) region are

$$\begin{aligned} \psi_0^-(s) &= \frac{s}{\tau_0^-} - \pi - 2 \arctan(\sinh \zeta), & r_0^-(s) &= \tau_0^- \sin \frac{s}{\tau_0^-}, \\ \varpi_0^-(s) &= 1 + (\tau_0^-)^2 \cos \frac{s}{\tau_0^-} - (\tau_0^-)^2, \end{aligned}$$

where  $\zeta = \sqrt{\tau_0^-/\varepsilon} (s - s_0^*)/\mu + \Gamma$  with  $\Gamma$  given by (4.3).

For the (+) region, they are

$$\begin{aligned} \psi_0^+(s) &= 2\pi - \frac{s_0^* - s}{\tau_0^+} - 2 \arctan(\sinh \eta), & r_0^+(s) &= \tau_0^+ \sin \frac{\widehat{s}_0 - s}{\tau_0^+}, \\ \varpi_0^+(s) &= -1 + (\tau_0^+)^2 - (\tau_0^+)^2 \cos \frac{\widehat{s}_0 - s}{\tau_0^+}, \end{aligned}$$

where  $\eta \equiv \sqrt{\tau_0^+}(s - s_0^*)/\mu + \Upsilon$  with  $\Upsilon$  given by (4.3).

The corresponding composite solutions at order  $\mu$  for the  $(-)$  region are

$$r_1^-(s) = \sqrt{\frac{\varepsilon}{\tau_0^-}} [2N \operatorname{sech} \zeta - 4M(1 + \tanh \zeta)],$$

$$\psi_1^-(s) = \frac{\tau_1^-}{(\tau_0^-)^2} s + \sqrt{\frac{\varepsilon}{\tau_0^-}} \left\{ \left[ 2A - \frac{4M}{r^*} - \left( \frac{6A1}{r^*} + \frac{\tau_1^-}{\sqrt{\tau_0^-}} \right) \zeta + \frac{4N}{r^*} \arctan(\sinh \zeta) + \frac{8M}{r^*} \ln(\operatorname{sech} \zeta) \right] \operatorname{sech} \zeta + \frac{2M}{r^*} \exp \zeta - \frac{6}{\tau_0^-} (1 + \tanh \zeta) \right\},$$

$$\varpi_1^-(s) = 2\tau_0^- \tau_1^- \left( \cos \frac{s}{\tau_0^-} - 1 \right) + \tau_1^- s \sin \frac{s}{\tau_0^-}.$$

In the above,  $M = [\cos(s_0^*/\tau_0^-)]/2$  and  $N = r^*/\tau_0^-$ .

For the  $(+)$  region

$$r_1^+(s) = \frac{1}{\sqrt{\tau_0^+}} [2T \operatorname{sech} \eta + 4P(1 - \tanh \eta)],$$

$$\psi_1^+(s) = \frac{\tau_1^+}{(\tau_0^+)^2} (\widehat{s}_0 - s) - \frac{\widehat{s}_1}{\tau_0^+} + \frac{1}{\sqrt{\tau_0^+}} \left\{ \left[ 2D - \frac{4P}{r^*} + \left( \frac{6P}{r^*} - \frac{\tau_1^+}{\sqrt{\tau_0^+}} \right) \eta + \frac{4T}{r^*} \times \arctan(\sinh \eta) + \frac{8P}{r^*} \ln(\operatorname{sech} \eta) \right] \operatorname{sech} \eta + \frac{2P}{r^*} \exp(-\eta) + \frac{6}{\tau_0^+} (1 - \tanh \eta) \right\},$$

$$\varpi_1^+(s) = 2\tau_0^+ \tau_1^+ \left( 1 - \cos \frac{\widehat{s} - s}{\tau_0^+} \right) + \tau_1^+ (\widehat{s}_0 - s) \sin \frac{\widehat{s}_0 - s}{\tau_0^+}.$$

In the above,  $P = -\{\cos[(\widehat{s}_0 - s_0^*)/\tau_0^+]\}/2$  and  $T = r^*/\tau_0^+$ .

The composite solutions for  $h^-$  and  $h^+$ , up to order  $\mu$ , are given by the corresponding inner solutions  $H_0/\mu + H_1 + \mu H_2$  described in the text.

#### REFERENCES

- AKIMOV, S. A., KUZMIN, P. I., ZIMMERBERG, J., COHEN, F. S. & CHIZMADZHEV, Y. A. 2004 An elastic theory for line tension at a boundary separating two lipid monolayer regions of different thickness. *J. Electroanal. Chem.* **564**, 13–18.
- ALBERTS, B., JOHNSON, A., LEWIS, J., RAFF, M., ROBERTS, K. & WALTER, P. 2002 *Molecular Biology of The Cell*, 4th edn. Garland Science, NY.
- ALLAIN, J.-M. & BENAMAR, M. 2006 Budding and fission of a multiphase vesicle. *Eur. Phys. J. E* **20**, 409–420.
- ALMEIDA, R. F. M., FEDOROV, A. & PRIETO, M. 2003 Sphingomyelin/phosphatidylcholine/cholesterol phase diagram: boundaries and composition of lipid rafts. *Biophys. J.* **85**, 2406–2416.
- BAUMGART, T., DAS, S. L., WEBB, W. W. & JENKINS, J. T. 2005 Membrane elasticity in giant vesicles with fluid phase coexistence. *Biophys. J.* **89**, 1067–1080.
- BAUMGART, T., HESS, S. T. & WEBB, W. W. 2003 Imaging coexisting fluid domains in biomembrane models coupling curvature and line tension. *Nature* **425**, 821–824.
- BENDER, C. M. & ORSZAG, S. A. 1999 *Advanced Mathematical Methods for Scientists and Engineers*. Springer.
- CALLADINE, C. R. & GREENWOOD, J. A. 2002 Mechanics of tether formation in liposomes. *ASME J. Biomech. Engng* **124**, 576–585.
- DAS, S. L. 2007 Studies of axisymmetric lipid bilayer vesicles: parameter estimation, micropipette aspiration, and phase transition. PhD Thesis, Cornell University.
- DUWE, H. P., KÄS, J. & SACKMANN, E. 1990 Bending elastic moduli of lipid bilayers: Modulation by solutes. *J. Phys. (Paris)* **51**, 945–961.

- EVANS, E. A. 1980 Minimum energy analysis of membrane deformation applied to pipet aspiration and surface adhesion of red blood cells. *Biophys. J.* **30**, 265–284.
- EVANS, E. & YEUNG, A. 1994 Hidden dynamics in rapid changes of bilayer shape. *Chem. Phys. Lipids* **73**, 39–56.
- HELFRICH, W. 1973 Elastic properties of lipid bilayers: theory and possible experiments. *Z. Naturforsch.* **28c**, 693–703.
- HINCH, E. J. 1991 *Perturbation Methods*. Cambridge University Press.
- ISRAELACHVILI, J. N. 1992 *Intermolecular and Surface Forces: With Applications to Colloidal and Biological Systems*, 2nd edn. Academic.
- JENKINS, J. T. 1976 Static equilibrium configurations of a model red blood cell. *J. Math. Biol.* **4**, 149–169.
- JENKINS, J. T. 1977 The equations of mechanical equilibrium of a model membrane. *SIAM J. Appl. Math.* **32**, 755–764.
- JÜLICHER, F. & LIPOWSKY, R. 1996 Shape transformations of vesicles with intramembrane domains. *Phys. Rev. E* **53**, 2670–2683.
- LEIBLER, S. 2004 Equilibrium statistical mechanics of fluctuating films and membranes. In *Statistical Mechanics of Membranes and Surfaces*, 2nd edn (ed. D. Nelson, T. Piran & S. Weinberg). Springer.
- LIPOWSKY, R., BRINKMANN, M., DIMOVA, R., HALUSKA, C., KIERFELD, J. & SHILLCOCK, J. 2005 Wetting, budding, and fusion—morphological transitions of soft surfaces. *J. Phys.: Cond. Mat.* **17**, S2885–S2902.
- LIPOWSKY, R. & SACKMANN, E., ed. 1995 *Structure and Dynamics of Membranes, Handbook of Biological Physics Vol. 1*. Elsevier.
- O'NEIL, B. 1966 *Elementary Differential Geometry*. Academic.
- POWERS, T. R., HUBER, G. & GOLDSTEIN, R. E. 2002 Fluid-membrane tethers: minimal surfaces and elastic boundary layers. *Phys. Rev. E* **65**, 041901–1–041908.
- SEIFERT, U. 1997 Configurations of fluid membranes and vesicles. *Adv. Phys.* **46**, 13–137.
- SEMRAU, S., IDEMA, T., HOLTZER, L., SCHMIDT, T. & STORM, C. 2007 Accurate determination of elastic parameters for multi-component membranes. arXiv:cond-mat/0612554v3.
- VEATCH, S. L. & KELLER, S. L. 2003 Separation of liquid mixtures in giant vesicles of ternary mixtures of phospholipids and cholesterol. *Biophys. J.* **85**, 3074–3083.
- VEATCH, S. L. & KELLER, S. L. 2005 Seeing spots: complex phase behavior in simple membranes. *Biochim. Biophys. Acta* **1746**, 172–185.
- WAUGH, R. & EVANS, E. A. 1979 Thermoelasticity of red blood cell membrane. *Biophys. J.* **26**, 115–132.
- WIDOM, B. 1999 Structure and tension of interfaces. *Molecular Phys.* **96**, 1019–1026.